Helium-atom-scattering measurements of surface-phonon dispersion curves of the C(111)-H(1×1) surface

Gerrit Lange and J. Peter Toennies
Max-Planck-Institut für Strömungsforschung, Bunsenstraße 10, D-37073 Göttingen, Germany
(Received 26 October 1995)

The surface-phonon dispersion curves of the hydrogen-terminated diamond (111)-(1×1) surface have been measured by inelastic helium-atom scattering. By using a very high incident-beam energy of 80.5 meV, the Rayleigh-wave dispersion curve could be observed throughout the entire Brillouin zone. The measured zone-boundary energies at the $\bar{M}$ point and $\bar{K}$ point are 64.4 and 70.6 meV, respectively. The data lie about 5% above the Rayleigh-wave dispersion curve obtained from semiempirical total-energy calculations.

The unique and special properties of diamond, such as extreme hardness, high chemical resistance, low friction coefficient, optical transparency over a wide spectral range, and large heat conductivity make it an ideal material for a variety of technical applications in mechanical, optical, and semiconducting devices. Technical use requires a high degree of material reproducibility which is not available with natural diamonds. For optimizing the synthesis of diamond by chemical vapor deposition (CVD), an understanding of elementary processes in diamond, especially its surfaces, is needed.

The (111) surface represents the most studied of single-crystal surfaces of diamond.[1] Most investigations of this crystallographic surface have focused on the role of hydrogen in the (1×1) to (2×1) phase transition. Different techniques such as low-energy electron diffraction (LEED),[2–5] medium-energy ion scattering,[4] or helium-atom scattering (HAS) (Ref. 6) have revealed a (1×1) symmetry for the hydrogen-saturated C(111) surface. Removing the hydrogen above ≈1300 K leads to a (2×1) phase of the clean surface[2–6] which is characterized by π-bonded chains of carbon atoms in the top layer.[7]

Studies of the lattice dynamics of the (111) surface of natural diamond as well as of diamond films grown by CVD have mainly been performed by high-resolution electron-energy-loss spectroscopy (HREELS).[8–15] For the (111) surface of natural diamond, Wachlawski *et al.*[8] and Lee and Apai[9] measured energy losses attributed to vibrations of different CH_n species or C-C stretching modes. Because the energy-loss spectra were recorded in the specular mode, energy losses at the $\bar{\Gamma}$ point of the surface Brillouin zone could only be observed. In a recent HREELS study on the (111) surface of a diamond film grown by the CVD technique, Aizawa *et al.*[10] observed the dispersion of energy losses in the off-specular mode originating from the Rayleigh wave. Very recently these authors published the complete phonon-dispersion curves for the $\bar{\Gamma}\bar{K}$ direction showing eight different modes on diamond films.[15] Due to experimental limitations of HREELS, only energy losses larger than about 20 meV with a resolution of 4–6 meV could be probed in their study.

Here we use inelastic HAS to measure the Rayleigh wave surface-phonon dispersion curves of the single-crystal C(111)-H(1×1) surface with a resolution of about 1.6 meV. Energy-loss features were observed up to 70.6 meV which are well above the previous HAS rough limit of about 30 meV.[16] This made it possible to follow the complete dispersion of the Rayleigh wave throughout the entire Brillouin zone. The experimental data are in qualitative agreement with very recently published semiempirical calculations of the surface-phonon spectrum of the hydrogen covered C(111)-(1×1) surface by Sandfort, Mazur, and Pollmann.[17]

The helium-atom-scattering apparatus has been described in detail in several previous reports.[16,18,19] Briefly, a highly monoenergetic helium-atom beam with a velocity spread of $\Delta v/v < 1\%$ is produced in a supersonic expansion and directed toward the crystal at an angle θ_i with respect to the normal. The scattered atoms are detected by a mass spectrometer which is located at the end of a 1.43-m flight tube with the angle between incoming and outgoing beams fixed at 90°. Different momentum transfers ΔK parallel to the surface are probed by rotating the sample around an axis normal to the scattering plane, thereby accessing different incident scattering angles θ_i and final angles θ_f. For time-of-flight experiments the helium beam is chopped with a variable-pulse-width rotating disc two-slit chopper. The present time-of-flight measurements were performed with an incident-beam energy of 80.5 meV, with an overall energy resolution of about 1.6 meV full width at half maximum (FWHM).

The C(111) crystal[20] [natural diamond, type-IIa, $4\times4\times0.25$ mm^3, <3° miscut from the (111) plane] was hand polished with 1-μm Al_2O_3 powder and afterwards with olive oil to produce the hydrogen-saturated surface. The sample was annealed *in situ* to about $T_s = 890$ K to remove residual atmospheric contaminations. The surface temperature was measured with an *in situ* calibrated NiCr/Ni thermocouple fixed on one of the two Mo clips which hold the sample to the manipulator with 6 degrees of freedom. The base pressure of the chamber was $<10^{-10}$ mbar with the target at 300 K, and $<10^{-9}$ mbar at 789 K.

Figure 1 shows typical angular distributions for two main symmetry directions of the surface Brillouin zone of the C(111)-H(1×1) surface, $[\bar{1}10]$ and $[\bar{1}2\bar{1}]$ for an incident wave vector of $k_i = 12.4$ Å^{-1} ($E_i = 80.5$ meV) at $T_s = 789$ K. At this elevated temperature and incident wave vector the

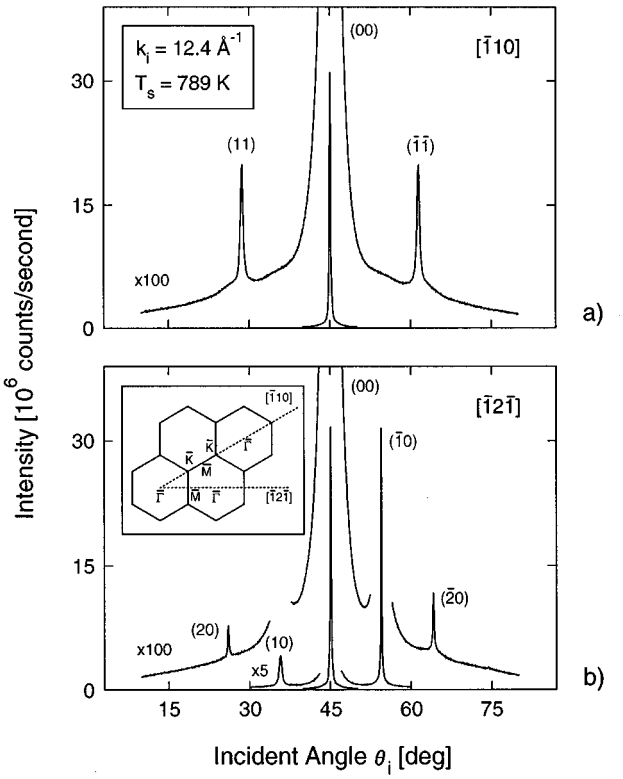

FIG. 1. Measured angular distributions of He atoms scattered from the C(111)-H(1×1) surface for (a) [$\bar{1}$10] and (b) [$\bar{1}\bar{2}\bar{1}$] azimuthal directions; incident wave vector $k_i = 12.4$ Å^{-1}; $T_s = 789$ K. The inset in (b) shows the reciprocal lattice of the C(111)-H (1×1) surface.

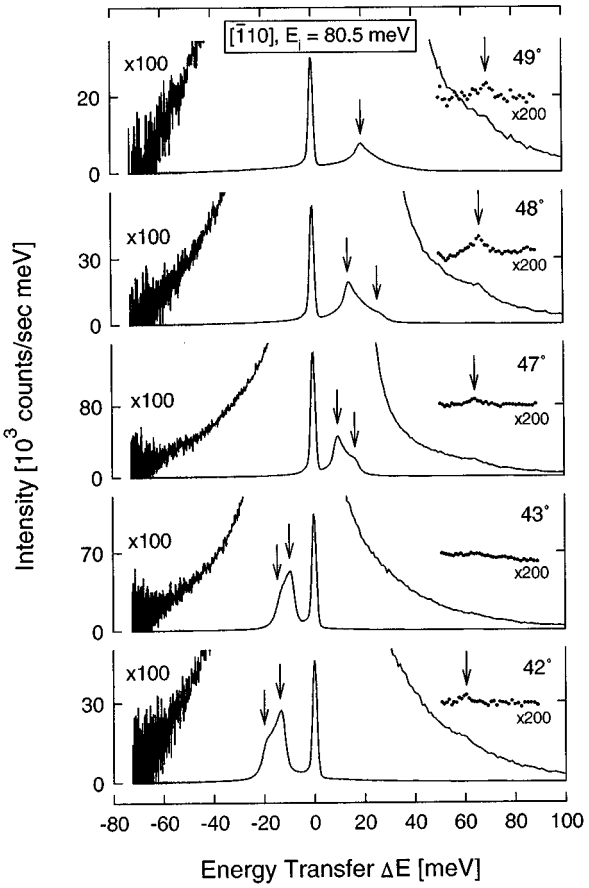

FIG. 2. Measured time-of-flight spectra for different incident angles along the [$\bar{1}$10] direction with $E_i = 80.5$ meV and $T_s = 789$ K. The arrows indicate the positions of single-phonon peaks.

diffracted intensities are attenuated by only about 20% compared to 300 K,[21] due to the large bulk Debye temperature of $\Theta_D = 2230$ K.[22]

Because of the small $<3°$ miscut, the sample surface contains steps leading to in-phase and out-of-phase conditions for the diffraction peaks depending on the perpendicular momentum transfer Δk_z. This is the reason that the FWHM of the (10) diffraction peak is larger than the ($\bar{1}$0) peak in Fig. 1(b). For the specular peak a maximum FWHM of 0.140 Å^{-1} was measured under out-of-phase conditions corresponding to a terrace length of at least 45 Å. Using a step height of 2.1 Å determined from the dependence of the specular intensity on the perpendicular momentum transfer Δk_z,[21] the actual miscut can be estimated to be 2.7°.

Time-of-flight spectra were measured for incident angles θ_i between 15° and 62° for the [$\bar{1}$10] direction, and between 28° and 58° for the [$\bar{1}\bar{2}\bar{1}$] direction, with $E_i = 80.5$ meV and $T_s = 789$ K. The collection times were between less than 1 and 5 h depending on the strength of the phonon peak intensities.

A typical series of time-of-flight measurements transformed to an energy-transfer scale along the [$\bar{1}$10] direction for different incident angles is presented in Fig. 2. Each curve shows, at $\Delta E = 0$ meV, an elastic scattered peak which is attributed to diffuse scattering from structural defects such as step edges. In addition to the elastic peak, phonon peaks (indicated by the arrows in Fig. 2) are present for both annihilation and creation. At a beam energy of 80.5 meV, phonon peaks on the creation side ($\Delta E < 0$ meV) are only observable up to energy transfers of about 50 meV. At larger energy transfers only weak annihilation events can be seen in the enlarged plots of Fig. 2. All single-phonon peaks are significantly broadened compared to the elastic peak because of the reduced surface transfer width because of the surface terraces.

The large Rayleigh-wave zone-boundary energy requires the use of a relatively high incident-beam energy to enhance the phonon excitation probability, and a high T_s to increase the density of phonon states.[16] The large surface Debye temperature Θ_D has the effect that both the beam energy and the surface temperature can be raised, compared to most previous experiments on more typical substances, without a deleterious effect from a multiphonon background. This can be understood from the Weare criterion[23]

$$\beta = \frac{M_{\text{beam}}}{M_{\text{surface}}} \frac{(E_{iz} + D) T_s}{k_B \Theta_D^2} \leqslant 0.01, \tag{1}$$

where E_{iz} is the perpendicular incident energy, D is the well depth, and Θ_D is an effective Debye temperature. β should be chosen close to, but less than, 0.01 to assure a good signal without a large multiphonon background. In the present experiments $\beta = 0.03$ using $\Theta_{D,\text{bulk}}$ and $D = 9.4$ meV.[6] The present data are characterized by unusually intense phonon

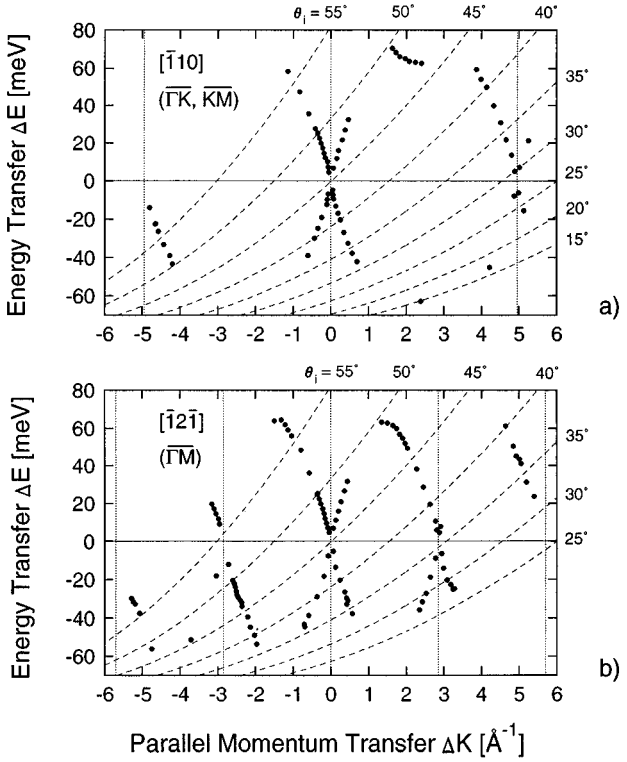

FIG. 3. Measured dispersion curves in an extended zone scheme for the main symmetry directions: (a) $[\bar{1}10]$ direction, reciprocal-lattice vector $G=4.99$ Å^{-1}. (b) $[\bar{1}2\bar{1}]$ direction, $G=2.89$ Å^{-1}; $E_i=80.5$ meV; $T_s=789$ K. The dashed lines show some typical scan curves at the indicated incident angles θ_i. $\Delta E>0$ corresponds to annihilation, and $\Delta E<0$ to creation events.

peaks, which is an indication of a steeply repulsive potential at the high incident energies.[24]

The energy and parallel momentum transfer of all measured phonon peaks are summarized in the extended zone diagram of Fig. 3 for the two main symmetry directions. Experimental scan curves showing the geometrical allowed parallel momentum transfers (ΔK) corresponding to the energy transfers (ΔE) are plotted as dashed lines. The scan curves intersect the zone-boundary phonons along the $\overline{KM}$ direction between 1.6 Å$^{-1}\leqslant\Delta K\leqslant$2.5 Å^{-1} at right angles making their observation particularly favorable despite their large energies [Fig. 3(a)]. The maximum energies at the zone boundaries are 64.4 meV at the $\bar{M}$ point and 70.6 meV at the $\bar{K}$ point. The maximum energy obtained for the $\bar{K}$ point lies slightly below the value of 72 meV recently measured by HREELS on a diamond film.[15]

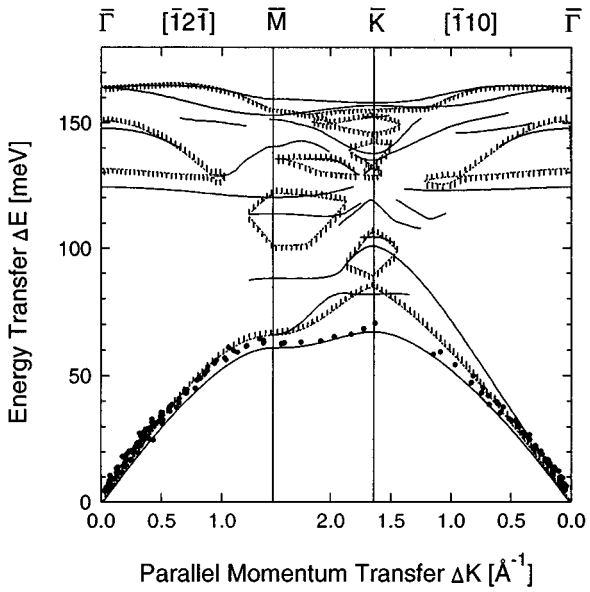

FIG. 4. Comparison of the present experimental data (●) and calculated surface dispersion curves (Ref. 17) (lines) in an irreducible zone.

The data from Fig. 3 were folded into the irreducible part of the first Brillouin zone, and are compared with the recently published calculations of the surface-phonon spectrum by Sandfort *et al.*[17] in Fig. 4. Our data lie consistently above the calculated Rayleigh-wave dispersion curve for both the $\overline{\Gamma M}$ and $\overline{\Gamma K}$ directions, with a deviation at both the $\bar{M}$ and $\bar{K}$ points of about 5%. Better agreement is observed along the $\overline{KM}$ direction. Those surface modes predicted to lie above the Rayleigh wave have energies too large to be detected with the present experimental conditions.

In summary, high-resolution helium-atom scattering has been used to study the Rayleigh-wave surface-phonon dispersion of the hydrogen-saturated C(111)-(1×1) surface. In these measurements the previous rough upper limit on HAS phonon energies has been extended from about 30 to 70.6 meV, and therefore it was possible to follow the Rayleigh wave over the entire Brillouin zone. The experimental Rayleigh-wave dispersion curve lies about 5% above a recent semiempirical calculation, and about 2% below HREELS measurements on diamond films. The agreement in both cases is considered to be very satisfactory.

We thank T. Schaich for help during the early stage of the experiment, and M. Buck, T. Schaich and Ch. Wöll for loan of the diamond sample and for discussions concerning the sample preparation.

[1] B. B. Pate, Surf. Sci. **165**, 83 (1986).
[2] J. J. Lander and J. Morrison, Surf. Sci. **4**, 241 (1966).
[3] P. G. Lurie and J. M. Wilson, Surf. Sci. **65**, 453 (1977).
[4] T. E. Derry, L. Smit, and J. F. van der Veen, Surf. Sci. **167**, 502 (1986).
[5] A. V. Hamza, G. D. Kubiak, and R. H. Stulen, Surf. Sci. **206**, L833 (1988).
[6] G. Vidali and D. R. Frankl, Phys. Rev. B **27**, 2480 (1983).
[7] K. C. Pandey, Phys. Rev. B **25**, 4338 (1982).
[8] B. J. Wachlawski, D. T. Pierce, N. Swanson, and R. J. Celotta, J. Vac. Sci. Technol. **21**, 368 (1982).
[9] S. T. Lee and G. Apai, Phys. Rev. B **48**, 2684 (1993).
[10] T. Aizawa, T. Ando, M. Kamo, and Y. Sato, Phys. Rev. B **48**, 18 348 (1993).

[11] B. Sun, X. Zhang, Q. Zhang, and Z. Lin, Appl. Phys. Lett. **62**, 31 (1993).
[12] B. Sun, X. Zhang, and Z. Lin, Phys. Rev. B **47**, 9816 (1993).
[13] B. Sun, X. Zhang, Q. Zhang, and Z. Lin, J. Appl. Phys. **73**, 4614 (1993).
[14] B. D. Thoms, P. E. Pehrsson, and J. E. Butler, J. Appl. Phys. **75**, 1804 (1994).
[15] T. Aizawa, T. Ando, K. Yamamoto, M. Kamo, and Y. Sato, Diamond Relat. Mater. **4**, 600 (1995).
[16] J. P. Toennies, in *Surface Phonons*, edited by W. Kress and F. W. de Wette (Springer, Berlin, 1991).
[17] B. Sandfort, A. Mazur, and J. Pollman, Phys. Rev. B **51**, 7150 (1995).
[18] G. Brusdeylins, R. B. Doak, and J. P. Toennies, Phys. Rev. B **27**, 3662 (1983).
[19] J. P. Toennies and R. Vollmer, Phys. Rev. B **44**, 9833 (1991).
[20] DRUKKER INTERNATIONAL, Beversestraat 20, 5431 SH Cuijk, The Netherlands.
[21] G. Lange, T. Schaich, J. P. Toennies, and C. Wöll (unpublished).
[22] C. Kittel, *Introduction to Solid State Physics* (Wiley, New York, 1971).
[23] J. H. Weare, J. Chem. Phys. **61**, 2900 (1974).
[24] D. Eichenauer, U. Harten, J. P. Toennies, and V. Celli, J. Chem. Phys. **86**, 3693 (1987).